Realistic Soil Modeling in Transient Analysis: Effects of Frequency Dependence, Water Content, Porosity and Stratification on Lightning Overvoltages

T. F. G. Pascoalato, A. R. J. de Araújo, S. Kurokawa, M. T. Correia de Barros

***Abstract*—This is an application paper examining the impact of incorporating water content, porosity, stratification, and frequency-dependent soil parameters on lightning-induced overvoltages in transmission lines (TLs). The authors implemented the Universal Line Model (ULM) in ATP-EMTP, following a previously proposed procedure, and developed MATLAB code using Wise's formulation for ground-return parameters. This approach enables more realistic soil modeling through three models: frequency-dependent parameters (Alípio-Visacro), wet and porous soils (Archie's law), and stratified soil (Xue's formulation). The study compares results obtained using ULM in ATP-EMTP with the software's built-in model, which relies on Carson's formulation, a more conservative method that neglects displacement currents and assumes constant soil conductivity. Overvoltages were analyzed in two parallel TLs, 50 meters apart, operating at 230 kV and 115 kV, with lightning striking the outer phase of the 230 kV line. The findings show significant differences between modeling approaches, particularly in induced overvoltages on non-struck phases. The results highlight the importance of using advanced soil models in transient analysis to enhance accuracy in estimating lightning overvoltages. Future ATP-EMTP versions should incorporate these models to improve simulation precision.**

***Keywords*—Frequency dependence, porosity, soil parameters, soil stratification, transmission lines, water content.**

I. Introduction

An appropriate soil model is essential for accurately evaluating the power systems performance, as electromagnetic transients are considerably influenced by the local soil characteristics. The soil consists of organic matter, moisture, and minerals, either homogeneous or stratified. In terms of its electromagnetic properties, the soil is characterized by the conductivity (σ) or the resistivity ($\rho = 1/\sigma$), the permittivity (ε), and the permeability (μ).

In electromagnetic transient studies and most EMTP simulation tools (ElectroMagnetic Transient Program), the soil has typically been modeled as a medium with frequency-constant electrical parameters. The conductivity (σ) is based on low-frequency measurements, the relative permittivity (ε) is generally chosen within the range of 2 to 40, depending on the soil's water content, while permeability (μ) is virtually invariant, typically taken as approximately that of free space ($\mu \approx \mu_0$) [1]. However, scientific literature indicates that both conductivity (σ) and permittivity (ε) are significantly affected by environmental factors such as water content, porosity, and temperature, as well as by the frequency of the electromagnetic field [2]. Additionally, most soils have a naturally stratified structure, a characteristic resulting from their formation process over several years.

This paper investigates overvoltages generated by a direct lightning strike using two distinct modeling approaches. In the first approach (referred to as the **Classic Approach**), the ULM implemented in the current version of ATP-EMTP [3] software (ATPDraw 7.5) is used. In this approach, the ground-return impedance is calculated using Carson's formulation, the soil conductivity being assumed as constant, and the displacement currents being neglected. In the second approach (referred to as the **Implemented Approach**), the TL is represented by the ULM employing the procedure proposed in [4] using the PCH file in the ATP-EMTP software. The main contribution of this paper is incorporation of realistic soil models, the ground-return impedance and admittance being computed based on Wise's formulation, considering: (i) frequency-dependent soil parameters as proposed by Alípio-Visacro [5], (ii) wet and porous soils based on Archie's law [6], and (iii) stratified soil using Xue's formulation [7]. By incorporating realistic soil modelling, engineers can achieve more reliable, safe, and cost-effective power system designs, improving overall operational efficiency and safety.

The paper is organized as follows: In Section II, the mathematical modeling of the per-unit-length parameters of the TL is presented. In Section III, the main models that calculate frequency-dependent soil parameters, water content, porosity and stratification are presented. Section IV addresses the methodology implemented by the authors in ATP-EMTP for considering more realistic soil modeling in the ULM. Section V presents a set of case studies under distinct modeling scenarios. Section VI presents the corresponding numerical results and discussions. Section VII concludes this article.

This work was supported by the Coordenação de Aperfeiçoamento de Pessoal de Nível Superior (CAPES)-Finance code 001 and by São Paulo Research Foundation (FAPESP) (grants: 2020/10141-4 and 2022/09182-3).
T. F. G. Pascoalato and S. Kurokawa are with São Paulo State University (UNESP), Ilha Solteira, Brazil. (E-mail of corresponding author: tfg.pascoalato@unesp.br). (E-mail: sergio.kurokawa@unesp.br); A. R. J. de Araújo is with University of Campinas, Campinas, Brazil. (E-mail: ajaraujo@unicamp.br); M. T. Correia de Barros is with IST, University of Lisbon, Lisbon, Portugal. (E-mail: teresa.correiadebarros@tecnico.ulisboa.pt).
Paper submitted to the International Conference on Power Systems Transients (IPST2025) in Guadalajara, Mexico, June 8-12, 2025.

II. Transmission line parameters

In a multiphase system of n phases, the longitudinal impedance and transversal admittance are expressed in matrix form $\boldsymbol{Z}_\ell(\omega)$ and $\boldsymbol{Y}_{\mathrm{t}}(\omega)$ $(n \times n)$, written as

$$\boldsymbol{Z}_\ell(\omega) = \boldsymbol{Z}_{\mathrm{int}}(\omega) + \frac{j\omega\mu_0}{2\pi}\left[\ln\left(\frac{D_{\mathrm{ij'}}}{d_{\mathrm{ij}}}\right) + \boldsymbol{S}_1\right], \quad (1)$$

$$\boldsymbol{Y}_{\mathrm{t}}(\omega) = j\omega\left\{\frac{1}{2\pi\varepsilon_0}\left[\ln\left(\frac{D_{\mathrm{ij'}}}{d_{\mathrm{ij}}}\right) + \boldsymbol{S}_2\right]\right\}^{-1}, \quad (2)$$

where $\omega = 2\pi f$ is the angular frequency [rad/s], f is the frequency [Hz], $\boldsymbol{Z}_{\mathrm{int}}(\omega)$ is the internal impedance [Ω/m] resulting from the *Skin Effect* on overhead conductors and is calculated using Bessel functions. The μ_0 is the vacuum magnetic permeability (μ_0 = $4\pi \times 10^{-7}$ [H/m]), $D_{\mathrm{ij'}}$ is the distance between the conductor i and the image of adjacent conductor j [m], d_{ij} is the distance between conductors i and j [m] and ε_0 is the vacuum permittivity (ε_0 = 8.85×10^{-12} [F/m]). The variables $\boldsymbol{S}_1$ and $\boldsymbol{S}_2$ are matrices derived from the Wise's work [8], [9], [10] to calculate the ground-return impedance and admittance. These are correction terms associated, respectively, to the magnetic and electric field in the soil. The matrices $\boldsymbol{S}_1$ and $\boldsymbol{S}_2$ derived from the Wise formulation can be calculated by the following equations [8], [9], [10]

$$\boldsymbol{S}_1 = 2\int_0^\infty \frac{e^{-(h_{\mathrm{i}}+h_{\mathrm{j}})\lambda}}{\sqrt{\lambda^2+\gamma_{\mathrm{g}}^2}+\lambda}\cos(r_{\mathrm{ij}}\lambda)d\lambda, \quad (3)$$

$$\boldsymbol{S}_2 = 2\int_0^\infty \frac{e^{-(h_{\mathrm{i}}+h_{\mathrm{j}})\lambda}}{\sqrt{\lambda^2+\gamma_{\mathrm{g}}^2}+\eta_{\mathrm{g}}^2\lambda}\cos(r_{\mathrm{ij}}\lambda)d\lambda, \quad (4)$$

where γ_{g}^2 and η_{g}^2 are given by [11]

$$\gamma_{\mathrm{g}}^2 = j\omega\mu_0[\sigma_{\mathrm{g}} + j\omega(\varepsilon_{\mathrm{r}} - k)\varepsilon_0], \quad (5)$$

$$\eta_{\mathrm{g}}^2 = \frac{\gamma_{\mathrm{m}}^2}{\gamma_0^2} = -\frac{j\omega\mu_0(\sigma_{\mathrm{g}} + j\omega\varepsilon_{\mathrm{r}}\varepsilon_0)}{\omega^2\mu_0\varepsilon_0}, \quad (6)$$

where h_{i} and h_{j} are the heights of the conductors i and j in relation to the ground level [m], r_{ij} is the horizontal distance between the conductors i and j [m], λ is an integration variable, σ_{g} is the soil conductivity [S/m] and ε_{r} is the relative permittivity. Note that k is a correction factor. If $k = 1$ in (5), the equations (3) and (4) are represented by Wise's formulation [8], [9], [10]. Otherwise, if $k = \varepsilon_{\mathrm{r}}$, the equation (3) is reduced to Carson's formulation [12].

III. Soil modeling

The soil conductivity σ_{g} and relative permittivity ε_{r} are frequency-dependent parameters [13]. The physical origin of this dependence is related to the various polarization processes which is associated to the losses that manifest in the medium along frequency [13]. In addition to frequency dependence, soil parameters are also affected by environmental factors such as water content, temperature, porosity, and chemical composition [1], [14]. Porosity is related to the volume of voids, or air gaps, present in the soil [15]. When the soil is saturated, these voids are filled with water, making the soil properties dependent on both porosity and water content. Additionally, most soils have a stratified structure. The stratification of the soil is the consequence of the biological, climatic, and geological processes over time. Horizontally stratified models are characterized by $(N-1)$ layers with finite conductivities and thicknesses, and the N-th layer, whose depth extends to infinity, representing the behavior of deep soil layer [16]. One of these techniques found in the literature to represent stratified soil is to perform an equivalence of the layers [7], [17], [18].

The adopted models for calculating soil parameters, which depend on frequency, water content, and porosity, and consider the soil as stratified, are presented below.

A. Frequency-dependent soil parameters

In 2014, Alípio and Visacro [5] proposed a semi-theoretical causal model to obtain frequency-dependent σ_{g} and ε_{r}. This model was developed based on results from various measurements, together with electromagnetic principles. The resulting expressions are given by [5]

$$\sigma_{\mathrm{g}}(f) = \sigma_0 + \sigma_0 \times h(\sigma_0)\left(\frac{f}{1\mathrm{MHz}}\right)^{\xi}, \quad (7)$$

$$\varepsilon_{\mathrm{r}}(f) = \frac{\varepsilon'_\infty}{\varepsilon_0} + \frac{\tan(\pi\xi/2)\times10^{-3}}{2\pi\varepsilon_0(1\mathrm{MHz})^\xi}\sigma_0 \times h(\sigma_0)f^{\xi-1}, \quad (8)$$

where, σ_0 is the soil conductivity [mS/m] at low frequencies (measured at 100 Hz), and the variables $h(\sigma_0)$, ξ, and $\varepsilon'_\infty/\varepsilon_0$ are given in Fig. 8 in [5].

B. Soil conductivity dependence on water content and porosity

Fu et al. [6] presented a model for the calculation of σ_{g} as a function of water content W and porosity ϕ. This model considers soil under dry and saturated conditions and also includes clay, sand, and silt contents. The proposed formulation is given by [6]

$$\sigma_{\mathrm{g}}(W,\phi) = \sigma_{\mathrm{dry}} + \left(\frac{\sigma_{\mathrm{sat}} - \sigma_{\mathrm{dry}}}{\phi^2} - \eta\right)W^2 + \eta\phi W, \quad (9)$$

$$\eta = \alpha\frac{\delta_{\mathrm{clay}}}{\delta_{\mathrm{sand}} + \delta_{\mathrm{silt}}} + \beta, \quad (10)$$

where, σ_{dry} and σ_{sat} are the soil conductivities in the dry and saturated states [S/m], respectively. The variable ϕ is the porosity [%] and W is the water content [%]. The δ_{clay}, δ_{sand}, and δ_{silt} characterize the volumetric fractions of clay, sand, and silt in the soil sample. The α and β are adjusted constants (α = 0.654 and β = 0.018) as described in [6].

C. Soil parameters considering a stratified soil

Xue et al. [7] presented a propagation constant equivalent method intended to approximate the parameters resulting from soil effects (ground-return impedance and admittance) of TLs located over a multilayered soil. Xue et al. used Wise's expressions for the impedance and admittance due to soil effects on TLs situated over homogeneous soil, along with the propagation constant equivalent method for stratified soils with

N layers. The equivalent propagation constant γ_{eq} obtained recursively for N-layered soil is given by [7]

$$\gamma_{eq} = \gamma_1 \frac{\gamma_1 + \gamma_{eq2,3} - (\gamma_1 - \gamma_{eq2,3})e^{-2|d_1|\gamma_1}}{\gamma_1 + \gamma_{eq2,3} + (\gamma_1 - \gamma_{eq2,3})e^{-2|d_1|\gamma_1}}, \quad (11)$$

$$\gamma_{eq2,3} = \gamma_2 \frac{\gamma_2 + \gamma_{eq3,4} - (\gamma_2 - \gamma_{eq3,4})e^{-2|d_2|\gamma_2}}{\gamma_2 + \gamma_{eq3,4} + (\gamma_2 - \gamma_{eq3,4})e^{-2|d_2|\gamma_2}}, \quad (12)$$

$$\gamma_{eq3,4} = \gamma_3 \frac{\gamma_3 + \gamma_{eq4,5} - (\gamma_3 - \gamma_{eq4,5})e^{-2|d_3|\gamma_3}}{\gamma_3 + \gamma_{eq4,5} + (\gamma_3 - \gamma_{eq4,5})e^{-2|d_3|\gamma_3}}, \quad (13)$$

$$\vdots$$

$$\gamma_{eqN\text{-}1,N} = \gamma_{N\text{-}1} \frac{\gamma_{N\text{-}1} + \gamma_N - (\gamma_{N\text{-}1} - \gamma_N)e^{-2|d_{N\text{-}1}|\gamma_{N\text{-}1}}}{\gamma_{N\text{-}1} + \gamma_N + (\gamma_{N\text{-}1} - \gamma_N)e^{-2|d_{N\text{-}1}|\gamma_{N\text{-}1}}}. \quad (14)$$

In (11)-(14), d_1, d_2 $\ldots$ $d_{N\text{-}1}$ are the depths of each layer, and γ_1, γ_2 $\ldots$ γ_N are obtained as [7]

$$\gamma_1 = \sqrt{\gamma_{e1}^2 - \gamma_0^2}, \quad \gamma_{N\text{-}1} = \sqrt{\gamma_{eN\text{-}1}^2 - \gamma_0^2}, \quad \gamma_N = \sqrt{\gamma_{eN}^2 - \gamma_0^2}, \quad (15)$$

where the propagation constants of each layer are

$$\gamma_{ek}^2 = j\omega\mu_k(j\omega\varepsilon_k + \sigma_k), \quad (1 \leq k \leq N). \quad (16)$$

To incorporate γ_{eq} into Wise's formulations, first, γ_g is replaced by γ_{eq} in (3) and (4). Then, γ_m is replaced by γ_{eq} in (6).

IV. Methodology

The most recent version of the ATP-EMTP software (ATPDraw 7.5) includes the implementation of the ULM model [3]. However, this implementation has some limitations, such as the ground-return impedance being calculated using Carson's formulation, the ground-return admittance and displacement currents being disregarded, and the soil conductivity being considered a constant parameter. Users cannot modify these characteristics in ATP-EMTP. To overcome these limitations, a procedure was proposed in [4] and updated in [19], in which the Universal Line Model (ULM) is implemented, combining the use of MATLAB software with the ATP-EMTP. In MATLAB, the user inserts the TL data using a graphical interface developed in the GUIDE environment. The associated code is responsible for calculating the line parameters, time delays, and rational approximation with Vector Fitting on the characteristic admittance and propagation function, resulting into a text file. In ATP-EMTP software, a foreign model reads the text file, a circuit is assembled using the type-94 component. This procedure allows the displacement currents, ground-return admittance, and frequency dependence of soil parameters can be considered.

In this work, the procedure described in [19] was followed by the authors, however, some modifications were implemented. Firstly, the GUIDE environment in MATLAB was not used; instead, the TL parameters, time delays, and Vector Fitting of the characteristic admittance and propagation function were written as a programming code in MATLAB. This procedure allows different soil models to calculate the ground-return parameters and, additionally and more importantly, to account for a more realistic soil, where not only the frequency dependence of the soil parameters but also water content, porosity, and stratification can be incorporated. Then, a data file is generated which is fully compatible with current version of ATP-EMTP (version ATPDraw 7.5). The PCH component is used to assemble an equivalent circuit, and thus, the transient responses are obtained directly in time domain.

Therefore, to calculate the transient lightning voltages, two approaches are employed:

- **Classic Approach:** For the line model, the ULM is used, which is available in the latest version of the ATP-EMTP software (version ATPDraw 7.5). In this approach, the soil impedance is calculated using Carson's formulation, and the soil admittance is neglected. Regarding the soil parameters, the relative permittivity is not explicitly considered in Carson's equation. By ignoring displacement currents, the model simplifies the soil as a purely conductive medium. Additionally, the soil conductivity is considered constant.
- **Implemented Approach:** For the line model, the ULM was implemented by the authors using MATLAB and ATP-EMTP software, following the procedure described in [4]. Since Carson's formulation does not allow for frequency-dependent soil parameters or provide a formulation for calculating ground-return admittance, the Wise formulation was used. In this approach, the soil parameters are dependent on frequency, water content, porosity, and soil stratification. To adjust the characteristic admittance and propagation function, 20 poles were used.

V. Case Study

To investigate the influence of considering the soil with more realistic characteristics, in computing direct lightning overvoltages, the system depicted in Fig. 1 is considered.

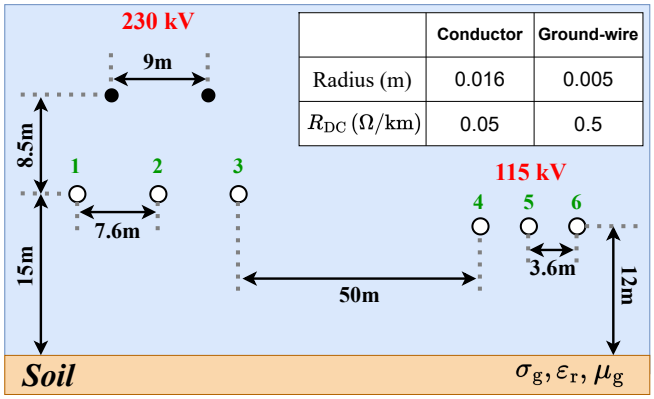

	Conductor	Ground-wire
Radius (m)	0.016	0.005
R_{DC} (Ω/km)	0.05	0.5

Fig. 1. Case study: 230 kV and 115 kV overhead TLs running in parallel.

In this configuration, two 10 km-length three-phase lines are running in parallel: A 230-kV three-phase TL with two ground wires, and a 115-kV three-phase line with no ground wires. In this previously used configuration [20], [4]. Phase 1 of the sending terminal (S) of the 230-kV three-phase TL is struck by a lightning, and the resulting overvoltages at

the receiving ends of both TLs are analyzed. The sending terminals (S) 2 and 3 are short-circuited. The receiving terminals (R) are open-circuited. The 115-kV three-phase TL has its three sending terminals (S) short-circuited and all receiving terminals (R) left open, as shown in Fig. 2.

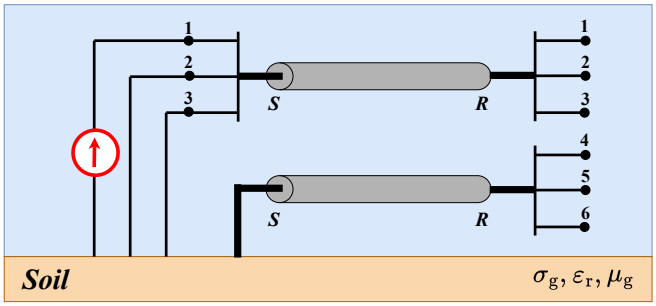

Fig. 2. Lightning striking phase 1 of the 230-kV TL.

Lightning is modeled as a currente source representative of the *first stroke*, mathematically given by a sum of the Heidler's functions given by [21]

$$i(t) = \sum_{k=1}^{p} \frac{I_{0k}}{\eta_k} \frac{\left(\frac{t}{\tau_{1k}}\right)^{n_k}}{1 + \left(\frac{t}{\tau_{1k}}\right)^{n_k}} e^{\frac{-t}{\tau_{2k}}}, \tag{17}$$

$$\eta_k = e^{\left[-\left(\frac{\tau_{1k}}{\tau_{2k}}\right)\left(n_k \frac{\tau_{2k}}{\tau_{1k}}\right)\right]^{\frac{1}{n_k}}}, \tag{18}$$

where, I_{0k} is the peak value of the current [A], τ_{1k} is the front time constant [s], τ_{2k} is the decay time constant [s], n_k is a coefficient related to the waveform slope, η_k is a peak correction factor, and p is the number of terms. The lightning current source is composed of a sum of 7 Heidler's functions (p = 7), with the parameters used for the simulations provided in Table 1 in [21]. The waveform of the lightning current representative of the *first return stroke* in the time domain is shown in Fig. 3. The frequency range from 10^{-1} Hz to 10^{7} Hz is used. The soil permeability is considered equal to that of vacuum.

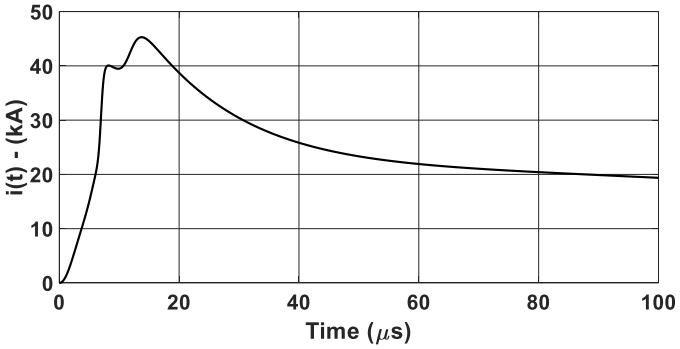

Fig. 3. Lightning current representative of the first return stroke.

Three cases were considered, comparing the Classic Approach with the Implemented Approach in all cases:

- *Case 1 - Influence of frequency-dependent soil parameters:* This case analyzes the transient voltages by comparing the Classic Approach with constant σ_g and the Implemented Approach with frequency-dependent soil parameters ($\sigma_g(f), \varepsilon_r(f)$), calculated using equations (7) and (8). The value of 0.0004 S/m was used for σ_g in the Classic Approach and for σ_0 in the Implemented Approach, as recommended in [1], where it is considered mandatory for soil parameters to be frequency-dependent for soils with conductivity less than 0.00142 S/m (700 Ω.m). Additionally, the literature indicates that more pronounced differences are observed in less conductive soils [4], [1]. It is worth noting that considering frequency-dependent soil parameters using the ULM model has already been addressed in [4]. However, since this work aims to demonstrate the influence of soil with more realistic characteristics using the ULM implementation, frequency dependence could not be excluded due to its importance.
- *Case 2 - Influence of water content and porosity:* This case analyzes the transient voltages by comparing the Classic Approach with constant σ_g and the Implemented Approach with soil conductivity dependent on water content and porosity ($\sigma_g(W, \phi)$), calculated using equation (9). The value of 0.0004 S/m was used for σ_g in the Classic Approach. For the Implemented Approach, a sand soil was considered, with parameters $\delta_{clay} = 5$, $\delta_{sand} = 90$, $\delta_{silt} = 5$, $\sigma_{dry} = 0.0004$ S/m, and $\sigma_{sat} = 0.04$ S/m [22], with 15% water content and 30% porosity. Using the (9), the calculated σ_g is equal to 0.011479 S/m. Additionally, a typical value of $\varepsilon_r = 10$ was assigned, representative of saturated sand soils [23]. The value of 0.0004 S/m for σ_g corresponds to a dry soil with no water content or porosity [22].
- *Case 3 - Influence of soil stratification:* This case analyzes the transient voltages by comparing the Classic Approach with constant σ_g equal to 0.0004 S/m and the Implemented Approach considering a stratified soil with 4 layers, where the equivalent propagation constant is obtained from equations (11)-(14). The values of σ_g, ε_r, and layer depths are based on the studies [17], [24], [25]. In this paper, the soil conductivities of the first, second, and third layers, as well as the thickness of all layers, were maintained as in these studies. However, only the last layer was assigned a soil conductivity of 0.0004 S/m, as shown in Table I. The value of 0.0004 S/m for σ_g in the Classic Approach is equal to the last layer conductivity. As stated in the literature, the contribution of each layer is approximately proportional to its thickness [26], which suggests that the final layer, with infinite thickness, exerts the greatest influence on the transient responses.

TABLE I
SOIL CONDUCTIVITIES, RESISTIVITIES, AND DEPTH OF EACH LAYER.

	Layer 1	Layer 2	Layer 3	Layer 4
σ_g [S/m]	0.004255	0.00028	0.004878	0.0004
ρ_g [Ω.m]	235.0	3571.43	205.0	2500.0
d [m]	1.2	5.33	21.06	∞

VI. Results and discussions

The overvoltages were obtained at the receiving terminals (R) of the 6 phases, considering the Classic Approach and the Implemented Approach. Results are depicted in Figs. 4 to 6, for the different cases. To highlight the influence of including more realistic soil models, the percentage differences of the peak voltage were computed.

Case 1: Influence of frequency-dependent soil parameters

Fig. 4 depicts the transient voltages obtained for Case 1. Results shown that the transient voltages for phase 1 (Fig. 4-(a)) obtained from both approaches are in good agreement during the initial time instants. However, for phases 2 and 3 (Figs. 4-(b), (c)), a pronounced difference between the two approaches can be observed, mainly at the peaks of the waveforms, as time progresses. The induced transient voltages (Figs. 4-(d), (e), (f)) exhibited even greater differences between the two approaches. The Implemented Approach produced transient voltages with attenuated peak values due to increased soil conductivity as frequency rises, and the higher attenuation constant in the propagation function when the frequency dependence of the soil is considered [11].

Case 2: Influence of water content and porosity

The transient voltages obtained for Case 2 are shown in Fig. 5. Results show that the differences between the two approaches are highly pronounced for all phases. In general, the transient voltages obtained using the Implemented Approach exhibited stronger attenuation and distortion compared to those assessed with the Classic Approach, as both the soil conductivity and the relative permittivity increase with the higher water content in the soil [14]. In this scenario, the soil conductivity is significantly higher (0.011479 S/m) when the water content and porosity are considered, compared to the conductivity of dry soil, which is assumed to be constant (0.0004 S/m) in the Classic Approach, resulting in a 28.69 times increase. This increase is due to the presence and movement of dissolved ions in the water, as in wet and porous soils, water fills the void spaces, forming an interconnected network that facilitates the movement of dissolved ions [15]. Results also show that the voltages induced on the 115-kV TL (Figs. 5-(d), (e), (f)) exhibit higher attenuation compared to those on the 230-kV TL. These results highlight the significant impact of accurate soil modeling on transient responses.

Case 3: Influence of soil stratification

The transient voltages for Case 3 are illustrated in Fig. 6. Results in Fig. 6-(a) show that the voltages generated on the 230-kV TL exhibit similar behavior for both approaches during the initial moments. However, as time progresses, the differences become more pronounced. For the voltages shown in Figs. 6-(b) to 6-(f), the transient waveforms display significant distortion and attenuation, especially at the peaks. High-conductivity layers allow electromagnetic waves to pass through more easily but also absorb and dissipate more energy, resulting in increased attenuation. Conversely, low-conductivity layers offer greater resistance to current flow and cause more significant voltage drops and reflections at the boundaries. Additionally, the contribution of each layer to the overall attenuation is approximately proportional to its thickness [26]. In this scenario, the third layer, with a depth of 21.06 m, and the fourth layer, with infinite thickness, have the most significant impact on the transient responses, particularly affecting the induced voltages on the 115-kV TL.

Computation of the percentage differences

To quantify the influence of incorporating more realistic soil models, the peak percentage difference δ_{P} is calculated by

$$\delta_{\mathrm{P}} = \frac{V_{\mathrm{P}}^{\mathrm{Classic}} - V_{\mathrm{P}}^{\mathrm{Implemented}}}{V_{\mathrm{P}}^{\mathrm{Classic}}} \times 100\%, \tag{19}$$

where $V_{\mathrm{P}}^{\mathrm{Classic}}$ and $V_{\mathrm{P}}^{\mathrm{Implemented}}$ are the voltages at the first peak (black ellipse in the figures) calculated by the Classic and the Implemented approaches, respectively. The first peak was considered, as it olds the greatest relevance in transient analyses. The computed differences δ_{P} are shown in Table II. Results show significant differences for the induced voltages. The case with the most pronounced peak difference was Case 2, where the soil's porosity and water content were considered, resulting in a difference of up to 78%, while, in Cases 1 and 3, where frequency dependence and soil stratification were considered, the difference was 20% and 51%, respectively. This demonstrates how the Classic Approach is a more conservative method that overestimates voltage peaks.

TABLE II
Peak voltage differences (%).

Cases \ Phases	230 kV			115 kV		
	1	2	3	4	5	6
1	0.095	6.182	7.906	19.475	19.887	20.139
2	1.097	33.977	40.930	74.370	76.539	78.380
3	0.161	16.409	18.558	48.624	50.103	51.391

Additional cases considering different conductivities were performed so that conclusions could be written.

VII. Conclusion

This paper presented the implementation of the ULM using more realistic soil models, including frequency-dependent and environmental factors such as porosity, water content, and stratification (denoted as Implemented Approach). Results were compared with those generated with the newly implemented ULM in the software ATP-EMTP (denoted as Classic Approach) where soil with constant conductivity is considered. Overall, results obtained by the two approaches for the investigated lightning overvoltages showed significant differences, demonstrating the importance of including more realistic soil models.

When the frequency dependence of soil parameters was considered, difference arises because the frequency-dependent soil conductivity increases with the increasing frequency and which does not occur when a constant soil is considered. Regarding the porosity and water content factors in the soil, the difference occurs due to the fact that a soil considered dry is less conductive, and when porosity and

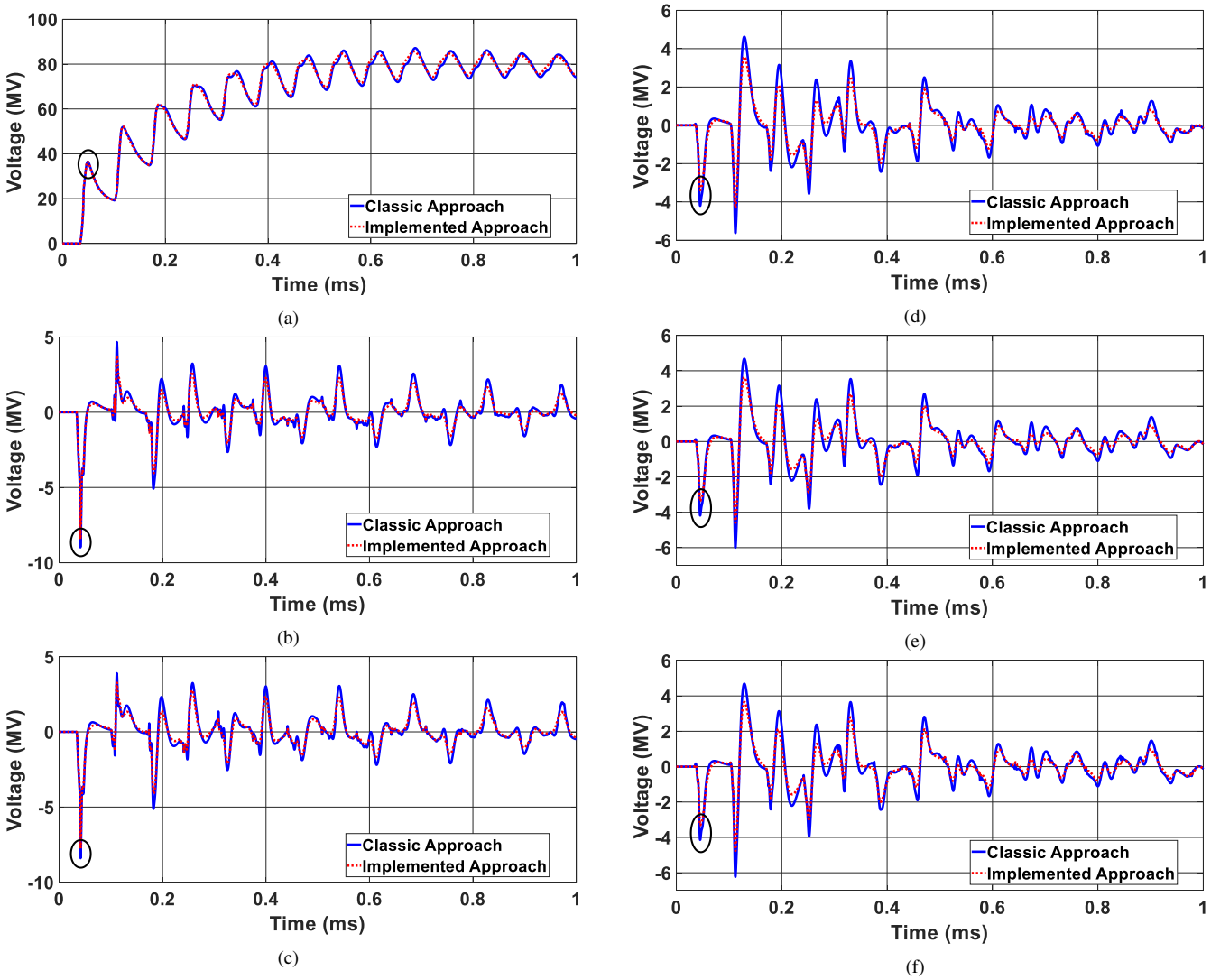

Fig. 4. Case 1: Transient voltages at the receiving ends obtained for the phases: (a) 1; (b) 2; (c) 3; (d) 4; (e) 5 and (f) 6.

water content are added, this conductivity tends to increase significantly. Concerning stratification, this occurs because the ULM Implemented Approach uses Xue's formula to represent a 4-layer soil in terms of a frequency-dependent equivalent propagation constant combined with Wise's formula to compute the ground-return parameters.

This article demonstrated that the realistic soil models notably impact the transient responses of a TL subjected to lightning strikes. Thus, accurate modeling of the ground is essential in transient analysis to ensure that all aspects of the power system's response during the transient events are correctly calculated.

VIII. Acknowledgement

Prof. Dr. Amauri Gutierrez Martins-Britto is acknowledged for the support and guidance during the implementation of the ULM in the software ATP-EMTP.

References

[1] W. G. CIGRE C4.33, "Impact of soil-parameter frequency dependence on the response of grounding electrodes and on the lightning performance of electrical systems," *Tech. Brochure 781*, pp. 1–66, 2019.

[2] Z. Li, J. He, B. Zhang, and Z. Yu, "Influence of frequency characteristics of soil parameters on ground-return transmission line parameters," *Electric Power Systems Research*, vol. 139, pp. 127–132, 2016, progress on Lightning Research and Protection Technologies.

[3] "The ATPDraw Simulation Software (2024), Version 7.5," https://www.atpdraw.net/, accessed: September 13, 2024.

[4] F. O. Zanon, O. E. Leal, and A. De Conti, "Implementation of the universal line model in the alternative transients program," *Electric Power Systems Research*, vol. 197, p. 107311, 2021.

[5] R. Alípio and S. Visacro, "Modeling the frequency dependence of electrical parameters of soil," *IEEE Transactions on Electromagnetic Compatibility*, vol. 56, no. 5, pp. 1163–1171, 2014.

[6] Y. Fu, R. Horton, T. Ren, and J. Heitman, "A general form of archie's model for estimating bulk soil electrical conductivity," *Journal of Hydrology*, vol. 597, p. 126160, 2021.

[7] H. Xue, J. Mahseredjian, A. Ametani, J. Morales, and I. Kocar, "Generalized formulation and surge analysis on overhead lines: Impedance/admittance of a multi-layer earth," *IEEE Transactions on Power Delivery*, vol. 36, no. 6, pp. 3834–3845, 2021.

[8] W. H. Wise, "Effect of ground permeability on ground return circuits," *The Bell System Technical Journal*, vol. 10, no. 3, pp. 472–484, 1931.

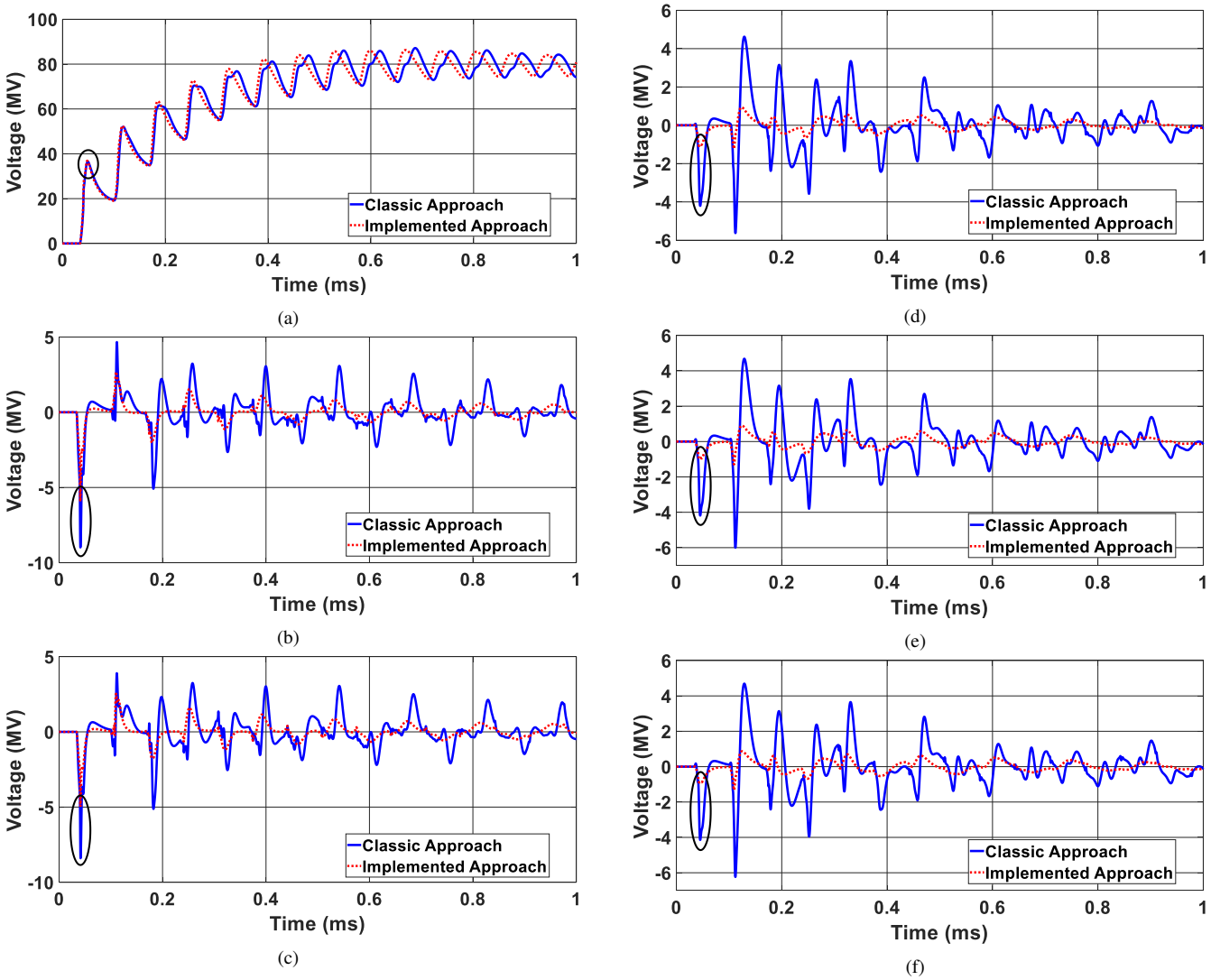

Fig. 5. Case 2: Transient voltages at the receiving ends obtained for the phases: (a) 1; (b) 2; (c) 3; (d) 4; (e) 5 and (f) 6.

[9] W. Wise, "Propagation of high-frequency currents in ground return circuits," *Proceedings of the Institute of Radio Engineers*, vol. 22, no. 4, pp. 522–527, 1934.

[10] W. H. Wise, "Potential coefficients for ground return circuits," *The Bell System Technical Journal*, vol. 27, no. 2, pp. 365–371, 1948.

[11] A. De Conti and M. P. S. Emídio, "Extension of a modal-domain transmission line model to include frequency-dependent ground parameters," *Electric Power Systems Research*, vol. 138, pp. 120–130, 2016.

[12] J. R. Carson, "Wave propagation in overhead wires with ground return," *The Bell System Technical Journal*, vol. 5, no. 4, pp. 539–554, 1926.

[13] S. Visacro and C. Portela, "Soil permittivity and conductivity behavior on frequency range of transient phenomena in electric power systems," in *Symp. High Voltage Eng.*, 1987.

[14] B. Salarieh, H. J. De Silva, and B. Kordi, "Electromagnetic transient modeling of grounding electrodes buried in frequency dependent soil with variable water content," *Electric Power Systems Research*, vol. 189, p. 106595, 2020.

[15] P. Teixeira, G. Donagemma, A. Fontana, and W. Teixeira, "Manual of soil analysis methods," *National Center for Soil Research, Embrapa: Rio de Janeiro, Brazil*, 2017.

[16] B. Zhang, X. Cui, L. Li, and J. He, "Parameter estimation of horizontal multilayer earth by complex image method," *IEEE Transactions on Power Delivery*, vol. 20, no. 2, pp. 1394–1401, 2005.

[17] A. G. Martins-Britto, F. V. Lopes, and S. R. M. J. Rondineau, "Multilayer earth structure approximation by a homogeneous conductivity soil for ground return impedance calculations," *IEEE Transactions on Power Delivery*, vol. 35, no. 2, pp. 881–891, 2019.

[18] J. S. Colqui, R. A. Moura, M. A. O. Schroeder, and J. Pissolato Filho, "Analysis of transmission line parameters considering multilayer soils," in *2022 IEEE XXIX International Conference on Electronics, Electrical Engineering and Computing (INTERCON)*. IEEE, 2022, pp. 1–4.

[19] O. E. S. Leal, and , A. De Conti and , F. O. S. Zanon, "User Manual ULM-ATP Version 3.2," accessed October 08, 2024. [Online]. Available: https://github.com/zanonfelipe/ULMAtp

[20] B. Gustavsen, "Modal domain-based modeling of parallel transmission lines with emphasis on accurate representation of mutual coupling effects," *IEEE transactions on power delivery*, vol. 27, no. 4, pp. 2159–2167, 2012.

[21] A. De Conti and S. Visacro, "Analytical representation of single-and double-peaked lightning current waveforms," *IEEE Transactions on Electromagnetic Compatibility*, vol. 49, no. 2, pp. 448–451, 2007.

[22] Y. Liu, Y. Jiang, Q. Gao, X. Li, G. Yang, Q. Zhang, and B. Tang, "Influences of soil water content and porosity on lightning electromagnetic fields and lightning-induced voltages on overhead lines," *Frontiers in Environmental Science*, vol. 10, p. 946551, 2022.

[23] J. B. Rhebergen, H. A. Lensen, P. B. Schwering, G. R. Marin, and J. M. Hendrickx, "Soil moisture distribution around land mines and the effect on relative permittivity," in *Detection and Remediation Technologies for Mines and Minelike Targets VII*, vol. 4742. International Society for Optics and Photonics, 2002, pp. 269–280.

[24] A. Ametani, "Stratified earth effects on wave propagation-frequency-dependent parameters," *IEEE Transactions*

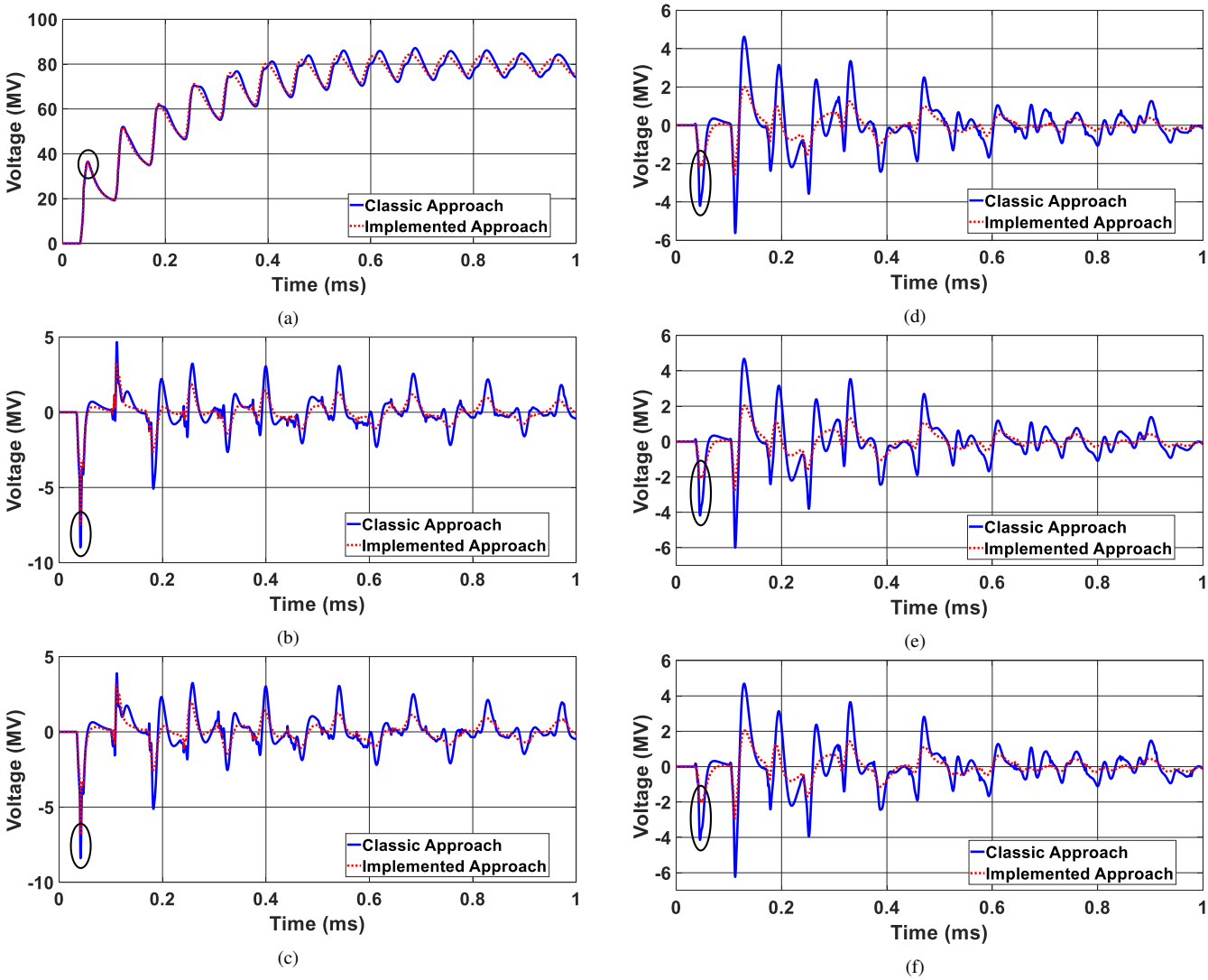

Fig. 6. Case 3: Transient voltages at the receiving ends obtained for the phases: (a) 1; (b) 2; (c) 3; (d) 4; (e) 5 and (f) 6.

on Power Apparatus and Systems, no. 5, pp. 1233–1239, 1974.

[25] J. He, R. Zeng, and B. Zhang, *Methodology and technology for power system grounding*. New Jersey: John Wiley & Sons, 2012.

[26] R. Southey and F. Dawalibi, "Improving the reliability of power systems with more accurate grounding system resistance estimates," in *Proceedings. International Conference on Power System Technology*, vol. 1. IEEE, 2002, pp. 98–105.